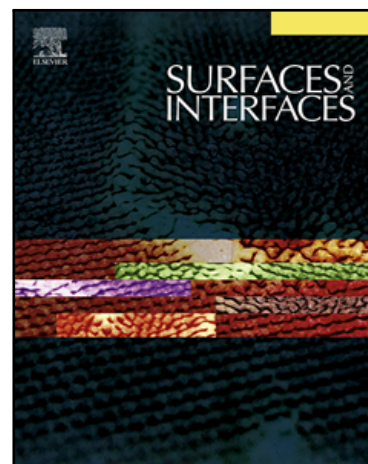


## Accepted Manuscript

Arachis hypogaea derived activated carbon/Pt catalyst: reduction of organic dyes

S. Anbu Anjugam Vandarkuzhali , S. Karthikeyan ,  
B. Viswanathan , M.P. Pachamuthu

PII: S2468-0230(18)30248-7  
DOI: [10.1016/j.surfin.2018.07.005](https://doi.org/10.1016/j.surfin.2018.07.005)  
Reference: SURFIN 222



To appear in: *Surfaces and Interfaces*

Received date: 21 June 2017  
Revised date: 26 July 2018  
Accepted date: 28 July 2018

Please cite this article as: S. Anbu Anjugam Vandarkuzhali , S. Karthikeyan , B. Viswanathan , M.P. Pachamuthu , Arachis hypogaea derived activated carbon/Pt catalyst: reduction of organic dyes, *Surfaces and Interfaces* (2018), doi: [10.1016/j.surfin.2018.07.005](https://doi.org/10.1016/j.surfin.2018.07.005)

This is a PDF file of an unedited manuscript that has been accepted for publication. As a service to our customers we are providing this early version of the manuscript. The manuscript will undergo copyediting, typesetting, and review of the resulting proof before it is published in its final form. Please note that during the production process errors may be discovered which could affect the content, and all legal disclaimers that apply to the journal pertain.

**Highlights**

- Agricultural waste: Groundnut shell utilized for activated carbon synthesis
- Synthesis and characterization of Pt nanoparticles on groundnut activated carbon was described
- Non-expensive catalyst Pt/AC: Reduction of different cationic and anionic dyes with  $\text{NaBH}_4$
- Short time ~2 min. dyes were reduced to its leuco forms

# Arachis hypogaea derived activated carbon/Pt catalyst: reduction of organic dyes

---

S. Anbu Anjugam Vandarkuzhali <sup>a</sup>, S. Karthikeyan <sup>b</sup>, B. Viswanathan <sup>a\*</sup>, M. P. Pachamuthu <sup>c\*</sup>

<sup>a</sup>*National Center for Catalysis Research, Indian Institute of Technology Madras, Chennai  
600036, Tamil Nadu, India*

<sup>b</sup>*European Bioenergy Research Institute, Aston University, Aston Triangle, Birmingham B4 7ET,  
United Kingdom*

<sup>c</sup>*Department of Chemistry, Bannari Amman Institute of Technology, Sathyamangalam, Erode  
638401, India*

\*Corresponding author. E-mail address: pachachem@gmail.com, pachamuthu@bitsathy.ac.in,  
Tel.: 04295 226306, +91 9944072620, fax: 04295 226666.

**Abstract**

Activated carbon from agro waste groundnut (*Arachis hypogaea*) shell was prepared by chemical activation and used as support for dispersion of 5% platinum nanoparticles. The Pt nanoparticles were obtained by the reduction in hydrogen gas medium. The synthesized groundnut activated carbon/platinum catalyst was characterized by various techniques such as X-ray powder diffraction, electron microscopies and X-ray photoelectron spectroscopy. The catalytic behaviour of the synthesized catalyst was investigated by exploring it as catalyst for the reduction of various classes of dyes; namely, triphenylmethane dyes such as Malachite green, phenol red and bromophenol blue, xanthene dyes: rose bengal, rhodamine 6G, rhodamine B, thiazine dye: methylene blue, azo dye: congo red and 4-nitrophenol by sodium borohydride in aqueous medium. Under suitable reaction conditions, for all tested dyes, cationic dyes were reduced at a faster rate than anionic dyes. The rate of reduction on the structure of dye and nature of catalyst was employed.

---

**Keywords:** *groundnut waste, carbon, platinum, reduction, dyes*

---

---

## 1. Introduction

Dyes and pigments are organic aromatic compounds used for imparting colors on various substrates such as textiles, plastic, leather, silk, paper, wool, jute, pharmaceutical, cosmetics and food. Generally, dyes are classified based on their nature, solubility, color and chemical structure [1, 2]. These organic dyes are well known industrial based environment pollutants. Discharge of these effluents contaminates the water bodies, thereby producing severe effects on aquatic animals and phytoplankton. Besides, these pollutants are known to cause health issues to human beings. To address this, so far, several methods (physical, chemical and biological) have been adopted for the removal of dyes from waste water [3, 4]. However, some disadvantages in the treatment process often compels for alternative environment friendly materials/methods that are efficient for commercial applications. The activated carbon (AC) is widely used as adsorbents and catalyst supports for the removal of various pollutants [3, 5-8]. Adsorption based removal of organic compounds over carbon materials, has been reported by various researchers, due to its excellent adsorption efficiency. In addition, large surface area, high porosity and structural homogeneity have directed different nanoparticles (Au, Ag, Cu, Co, Ni, Pd and Pt) dispersion on carbon materials. Most of these carbon supported nanoparticles have been successfully utilized for the removal of pollutants [9-15]. Particularly, Pt nanoparticles modified carbon supports have also been investigated for hydrogenation type reactions [16-18].

The conversion of agricultural waste materials into useful product promoting environmental protection reduces the production cost of useful materials. Various natural agro-wastes such as rice husk/stalk, grape stalk, saw dust, coconut husk/shell, jatropha curcas pods, bamboo, groundnut shell and sugarcane bagasse have been used as precursor for the production

of AC [19, 20]. Recently, Zhang *et al* have selected bio-wastes, including peanut shell, corncob powder, bagasse, grapefruit skin, walnut shell and straw powder as the precursors to prepare ACs by KOH activation to increase the surface area (upto 2484 m<sup>2</sup>/g) and to improve their electrochemical performance [21]. In particular, utilizing groundnut waste as renewable sources to produce AC product is of great interest, as India produces huge amount of groundnuts in the world. They have non-carbon constituents, which will retain most functional groups after carbonization [22, 23]. Hence, in the present work, synthesis of activated carbon from groundnut waste and Pt nanoparticles dispersions on AC are discussed. The performance of Pt/AC catalyst was tested for the dye hydrogenation reaction using sodium borohydride (NaBH<sub>4</sub>). Also, in order to understand whether the nature of the dyes influences the reduction process, both anionic (azo - congo red) and cationic (thiazine – methylene blue; xanthene - Rhodamine B, Rhodamine 6G) dyes have been selected as model environmental pollutants and their structural influence over reaction kinetics are also considered.

## 2. Material and methods

### 2.1 Preparation of groundnut activated carbon (AC)

Initially, the groundnut shell collected from groundnut oil industry (byproduct) and commercial market was washed to remove impurities and dried in sun light. The dried samples were grounded and sieved to get the mesh size of about 4 mm. The activating agent (KOH solution; 0.2 M) was mixed with sieved groundnut waste in selected ratio (1:1) and the mixture was continuously stirred for 5 h. To perform the carbonization process, the mixture was heated at 600 °C for 1 h under nitrogen atmosphere with the heating rate of 10 °C/min. The product was then cooled to room temperature under nitrogen atmosphere. The obtained carbon sample was

washed with dilute HCl solution and distilled water until the pH of the washing solution reached 7. The obtained sample was named as AC.

## 2.2 Preparation of Pt/AC catalyst

The Pt dispersion on AC was carried out by incipient wetness impregnation method using chloroplatinic acid ( $\text{H}_2\text{PtCl}_6 \cdot 6\text{H}_2\text{O}$ ) as precursor, the weight dispersed with AC was fixed to about 5 %. The mixture of AC (0.1 g) and  $\text{H}_2\text{PtCl}_6 \cdot 6\text{H}_2\text{O}$  (0.018 g) was stirred for 6 h at 60 °C. The resultant mixture was dried under vacuum. The dried sample was reduced inside tubular furnace with a ramp rate of 5 °C/min. and finally maintained at 200 °C for 1 h under hydrogen atmosphere. The final product was labelled as Pt/AC.

## 2.3 Material characterization

Powder X-ray diffraction (PXRD) was recorded on a Bruker D8 ADVANCE diffractometer, using Cu K $\alpha$  radiation ( $\lambda = 1.5418 \text{ \AA}$ ). FT-IR spectroscopy (Perkin-Elmer) was used for the investigation of surface functional groups in synthesized catalyst. Spectra analysis was recorded in the range of 4000 to 400  $\text{cm}^{-1}$  for 50 scans. The prepared AC sample (0.01 g) was mixed with spectroscopy grade KBr (0.1 g) in a mortar. The mixture was then pelletized as disks with dimensions of 1 mm in thickness; and 13 mm in diameter. Scanning electron microscopic (SEM) analysis was performed with a Philips XL-30 and High-resolution transmission electron microscopy (HRTEM) was performed with a Philips CM-300 high resolution system operating at 20 keV. X-ray photoelectron spectroscopy (XPS) measurements were carried on the VG Microtech 3000 Multilab. Atomic force microscopy (AFM) measurements were carried out using a multimode SPM from Digital Instruments with a Nanoscope IIIa controller. For AFM sample preparation, first Pt/AC sample prepared by (1

mg/10 mL DMF) and then sonicated sample was dropped on glass substrate and dried for AFM imaging. The liquid sample UV-Visible spectrum was recorded in the range of 200-800 nm with a Perkin Elmer spectrometer. Nitrogen adsorption-desorption isotherm was obtained at 77 K using a Micromeritics ASAP 2020 porosimeter. The specific surface area of the sample was calculated using the BET method (using the adsorption isotherm).

#### **2.4 Reduction of dyes using Pt/AC catalyst**

The selected dye solution ( $20 \text{ mg L}^{-1}$ ) and sodium borohydride (10 mmol) were taken in a quartz cell and purged with  $\text{N}_2$  gas. Typically, Pt/AC catalyst (5 mg) was added to the above mixture and the progress of the reduction reaction was monitored by recording the time-dependent absorbance spectra using a UV-Visible spectrophotometer at the respective chromophoric wavelength ( $\lambda_{\text{max}}$ ) of the dyes. For the recycling experiments, the catalyst was collected by decantation, washed, dried and reused for subsequent reduction reactions with fresh dye solutions.

#### **2.5 Reaction kinetic analysis**

The kinetics of the dye reduction reaction was studied by carrying out the experiments at room temperature with fixed amount of the dyes and catalyst. A pseudo unimolecular condition was maintained for the reduction reaction by adding excess of sodium borohydride compared to the dyes and catalyst [24, 25]. Previous Au nanoparticles supported carbon based catalyst reports revealed the same trends for reduction reactions by sodium borohydride [26, 27]. The rate constant was calculated from the slopes of the plots of  $\ln C_0/C$  vs time. The rate constants and dyes percentage reduction were calculated using the following mathematical expressions.

$$\bullet \quad \% \text{ reduction} = \frac{\text{O.D at initial time } (C_0) - \text{O.D. at time } t (C_t)}{\text{O.D at initial time } (C_0)} \times 100 \quad (1)$$

where,  $C_0$  = initial concentration of the dye solution

$C_t$  = concentration remaining after reaction at time  $t$

The Gibb's free energy of activation  $\Delta G^\ddagger$ , for the reduction process was calculated at 300 K using the following formula,  $\Delta G^\ddagger = -RT \ln k$  (2)

Where,  $k$  is the rate constant for the reduction reaction,  $R$  is universal gas constant (8.314 J mol<sup>-1</sup> K<sup>-1</sup>) and  $T$  is the absolute temperature in Kelvin.

## 2.6 The apparent kinetic rate constant ( $k_{app}$ ) determination

The apparent kinetic rate constant ( $k_{app}$ ) can be considered proportional to the total surface  $S$ , of all Pt nanoparticles [28]. Thus  $k_{app}$  can be defined as

$$\bullet \quad -\frac{dC_{dye}}{dt} = -k_{app} \cdot C_{dye} = -k S C_{dye} C_{BH_4} \quad \dots (3)$$

Where,  $C_{dye}$  and  $C_{BH_4}$  are the concentrations of adsorbed dye and NaBH<sub>4</sub>, respectively and  $k$  is the rate constant of the surface reaction. When sodium borohydride is in excess, eqn. (3) can be simplified into eqn. (4) and eqn. (5),

$$\bullet \quad -\frac{dC_{dye}}{dt} = -k_{app} \cdot C_{dye} \quad \dots (4)$$

$$\bullet \quad k_{app} = \frac{1}{t} \times \ln \frac{C_0}{C} \quad \dots (5)$$

where  $C_0$  is the initial dye concentration,  $C$  is the concentration at time  $t$ . The plots of  $\ln C_0/C$  vs time are derived and  $k_{app}$  is calculated from the slope.

### 3. Result and discussion

#### 3.1 Pt/AC catalyst characterizations

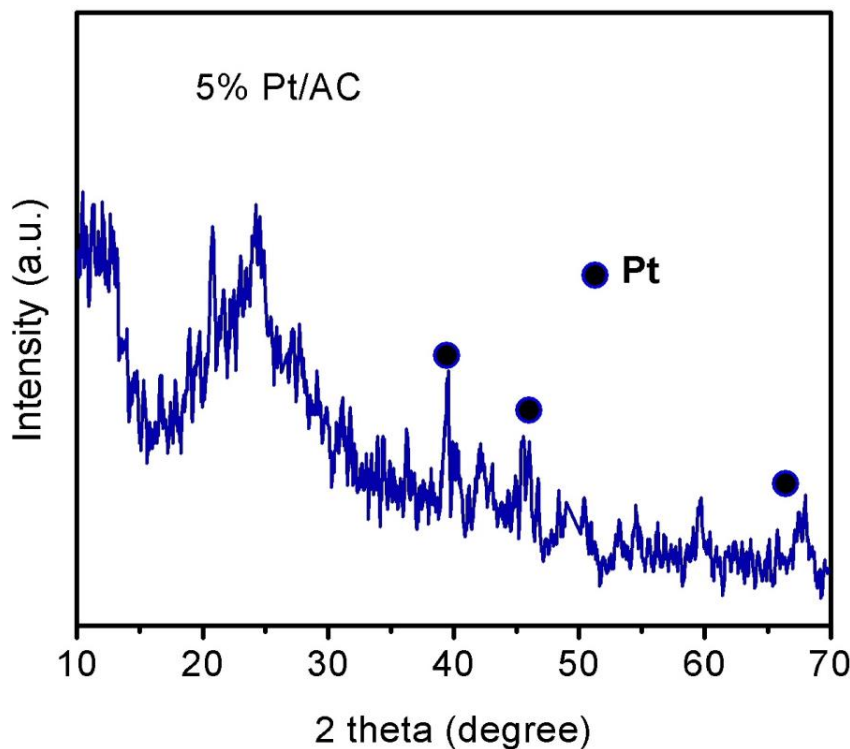


**Figure 1** PXRD pattern of Pt/AC catalyst

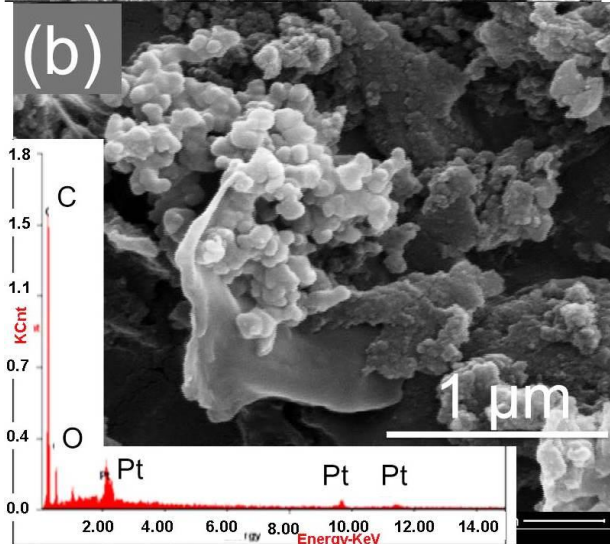
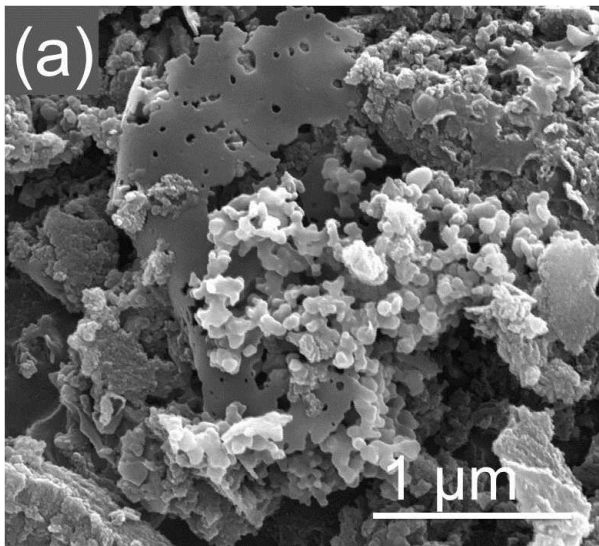
The crystalline nature of the as-synthesized Pt/AC catalyst was analyzed using PXRD measurements with  $2\theta$  values between  $10^\circ$  and  $70^\circ$ . PXRD pattern of Pt nanoparticles supported on AC was shown in **Fig. 1**. The diffraction peaks at  $2\theta$  values  $39.8^\circ$ ,  $46.2^\circ$  and  $67.5^\circ$  respectively correspond to the (111), (200) and (220) planes of Pt crystal which confirm the face-centered-cubic (fcc) lattice structure [29, 30]. A broad peak between  $15^\circ$  and  $30^\circ$  was related to the graphite structure of the synthesized AC support. The average crystalline size of the Pt nanoparticles was calculated using the (200) plane and was found to be 2.6 nm.

The surface morphology of the catalysts was analyzed using SEM and HRTEM microscopic images. **Fig. 2** displays the typical SEM and HRTEM images of Pt/AC catalyst. It can be seen that different shaped carbon spheres along with porosity exists in the sample (**Fig. 2**

(a, b)). The presence of Pt does not alter the nature of AC as evident from the porous, rough and finger-like structures of the surface. Further, Pt nanoparticles are spherical in shape and are homogeneously dispersed on the pores of the support AC (**Fig. 2 c, d**) in the range of 2-3 nm. The spherical Pt nanoparticles are encircled in white circles (**Fig. 2 d**). The mean size of the Pt nanoparticles was calculated to be 2.5 nm, which was in good agreement with PXRD results and the lattice fringe at 2.35 nm corresponds to the (111) plane of Pt nanoparticle.

In general, activated carbon contains pores on its surface which holds water during the preparation process. After the addition of the Pt precursor ( $\text{H}_2\text{PtCl}_6$ ), the  $\text{PtCl}_6^{2-}$  ions get adsorbed on the walls of the pores, as they are soluble in water present on pore walls. Since most of the reduction of precursor ions occurs on the walls, higher uniform dispersion of Pt nanoparticles was achieved. Also, AC possesses amphoteric nature, in which the basal plane edges of the carbon atoms with different hetero atoms, display the acidic and basic character of carbon surface. The presence of abundant hydrophilic groups (carboxyl, hydroxyl, carbonyl) on the surface of AC support facilitates the strong metal support (MS) interactions as evident from the uniform distribution of nanoparticles (**Fig. 2 d**). Similarly, the  $\pi$ -electron rich centers (basic sites) associated with the basal planes also contribute to strong MS interaction. These factors minimize aggregation thereby favors uniform dispersion of Pt nanoparticles as evident from SEM and HRTEM images [31].

The inserted EDAX spectrum (**Fig.2 b**) indicates the presence of C, O and Pt elements and their elemental compositions confirm the weight percentage of the Pt active site. The average amount of Pt present in the AC was estimated to be about 4.5 %. Further, the surface roughness, pores and Pt nanoparticle dispersions are illustrated using AFM images in **Fig. S1**.



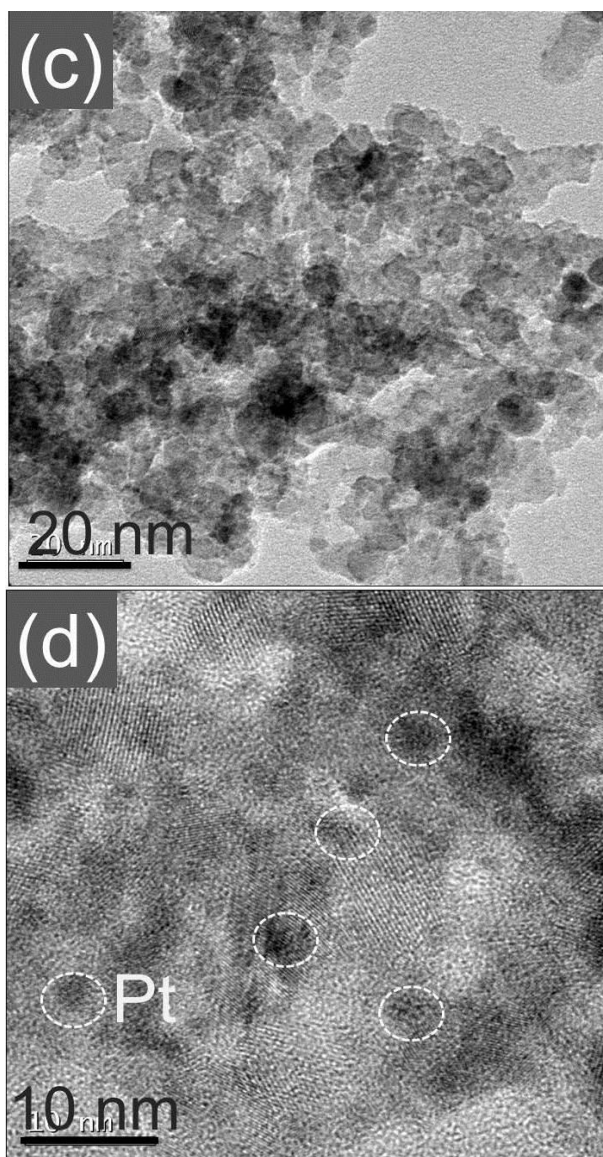


**Figure 2** (a, b) SEM images of Pt/AC (EDX inserted in bottom left) and (c, d) HRTEM images of Pt/AC catalyst

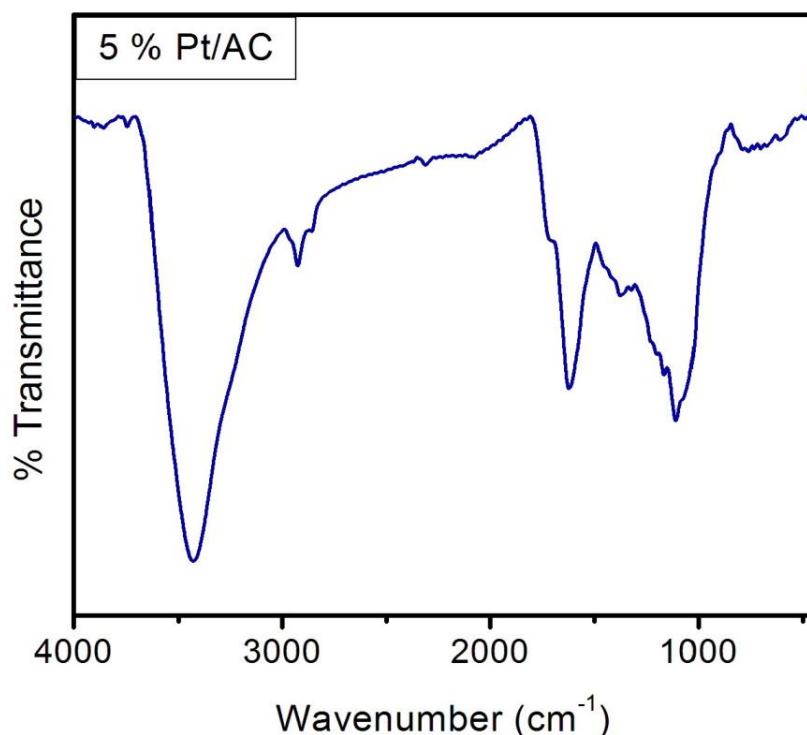
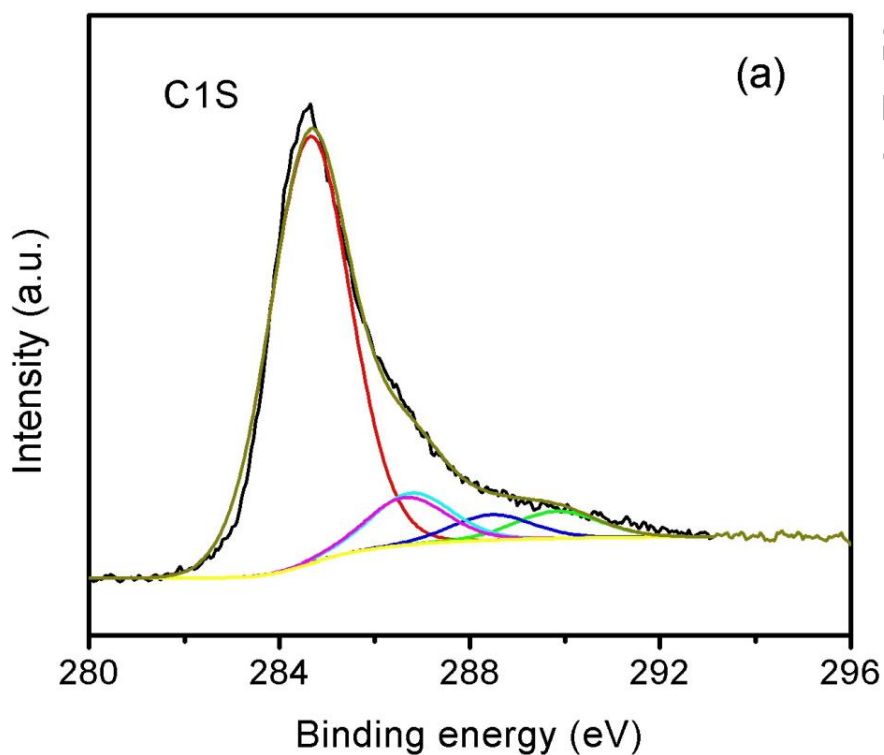


**Figure 3** FTIR spectrum of Pt/AC catalyst

BET isotherms were used to determine the surface area of Pt/AC catalyst. The extent of the surface area for adsorption and qualitative information on the adsorption process can be derived from the shape of the adsorption isotherm (not shown). The BET surface area of the prepared Pt/AC sample was found to be 956 m<sup>2</sup>/g (standard deviation 21.3), with pore volume of 0.4 cm<sup>3</sup>/g. Moreover, pure AC exhibits a surface area of 983 m<sup>2</sup>/g. Hence, the presence of higher surface area facilitates uniform dispersion of Pt and also contributes to higher adsorption property.

The surface functional groups in AC were analyzed using FTIR technique. **Fig.3** presents the FTIR spectrum for obtained Pt/AC catalyst. The broad band around 3400 cm<sup>-1</sup> is mainly caused by the O-H stretching vibration of the adsorbed water molecules and its bending vibration mode is observed at 1610 cm<sup>-1</sup>. The IR peak at 2925 cm<sup>-1</sup> is attributed to the stretching vibration of C-H bonds. Additionally, the bands observed at 1610 cm<sup>-1</sup>, 1440 cm<sup>-1</sup> and 1090 cm<sup>-1</sup> could be

assigned to C=O stretching, C=C vibration in aromatic and C-O stretching vibration of esters, respectively [21, 32]. However, some reports have mentioned the band at  $1092\text{ cm}^{-1}$  is due to –OCH<sub>3</sub> group present in the lignin structure, which was common for many adsorbents [33].



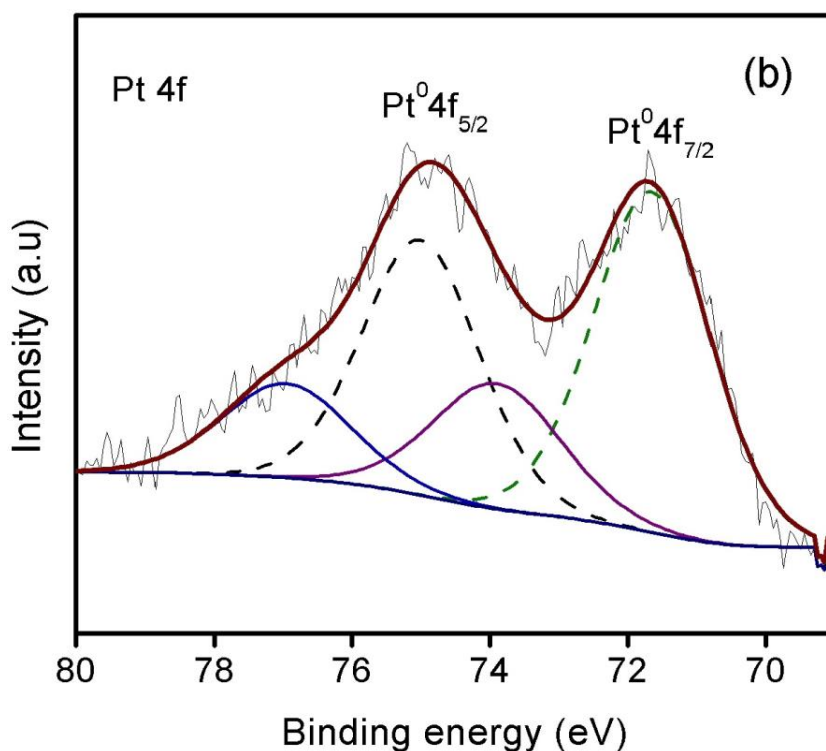


**Figure 4** (a) C1s and (b) Pt 4f core level XPS spectrum of Pt/AC catalyst

XPS was used to investigate the elemental composition of the surface and chemical states of the AC and Pt/AC samples. The XPS spectra with different binding energy (BE) ranges of Pt/AC catalyst were displayed in **Fig. 4**. The deconvoluted C1s spectrum (**Fig. 4 a**) of Pt/AC samples showed the peaks at 284.6, 286.2, 286.7, 287.8 and 289.0 eV, which are assigned to the  $sp^2$ -hybridised characteristic carbon (C-C, C-O & C-H). The BE at 284.6 eV is the most intense peak correlate to C-C group. The BE values at 286.2 eV and 286.7 eV, related to C-O bonds or amide functional groups in the porous carbon. Besides, the B.E values at 287.8 eV and 289 eV are due to carboxylic and ester functional groups, respectively [29, 32]. **Fig.4 b** represents the XPS spectrum of Pt 4f with a doublet corresponding to Pt  $4f_{5/2}$  and Pt  $4f_{7/2}$ . As can be seen, the intense peaks with BE values of 71.3 (Pt  $4f_{7/2}$ ) and 74.5 eV (Pt  $4f_{5/2}$ ) confirmed the presence of metallic Pt [15, 28, 29]. Besides, the low intense peaks at 72.4 and 75.8 eV could be assigned to

either Pt bonded to the AC or Pt oxides like PtO<sub>2</sub> and Pt(OH)<sub>4</sub>, respectively [34]. These results are consistent with the previous report [30].

### 3.2 Reduction of dyes using Pt/AC catalyst

The ability of Pt/AC as a catalyst was tested for the reduction of various classes of dyes by sodium borohydride under heterogeneous conditions at room temperature in aqueous medium. Generally, reduction of dyes is found to be thermodynamically favorable but kinetically unfavorable. In order to find if the sodium borohydride reduction is catalyzed by Pt/AC, experiments are conducted in the presence and absence of catalyst under normal conditions (pH ~ 7) and analyzed with UV-Vis spectrometer. It is noted that in the absence of Pt/AC, the  $\lambda_{\max}$  values of the dyes are not changed, which indicate the importance of catalyst and inability of NaBH<sub>4</sub> to independently reduce the dyes. Addition of catalytic amount of Pt/AC led to visible color change of the solution to colorless rapidly, which implied the formation of leuco form (reduced dye) during the reduction process.

#### 3.2.1 Effect of structural variations in dyes

The effects of structural variations on the reduction rate of dyes were studied by selecting triphenyl methane, xanthene, thiazine and azo dye as model compounds (**Fig. 5**). The group of selected dyes and their corresponding chromophoric absorbance ( $\lambda_{\max}$ , nm) values are summarized in **Table 1**.

**Table 1** Selected dyes, their examples, nature and UV-Visible absorbance wavelength

No.	Dyes	Nature	Selected dye	Chromophoric peaks
				( $\lambda_{\max}$ , nm) <sup>a</sup>
1.	Triphenyl methane	Cationic	Malachite green (MG)	617
		Anionic	Phenol red (PR)	557
		Anionic	Bromophenol blue (BPB)	592
2.	Xanthene	Cationic	Rhodamine B (RhB)	554
		Cationic	Rhodamine 6G (Rh 6G)	527
		Anionic	Rose Bengal (RB)	537
3.	Thiazine	Cationic	Methylene blue (MB)	665
4.	Azo	Anionic	Congo red (CR)	496
	Nitro		4-Nitrophenol (4-NP)	400

<sup>a</sup>Wavelength values obtained from the UV-Visible spectrum.

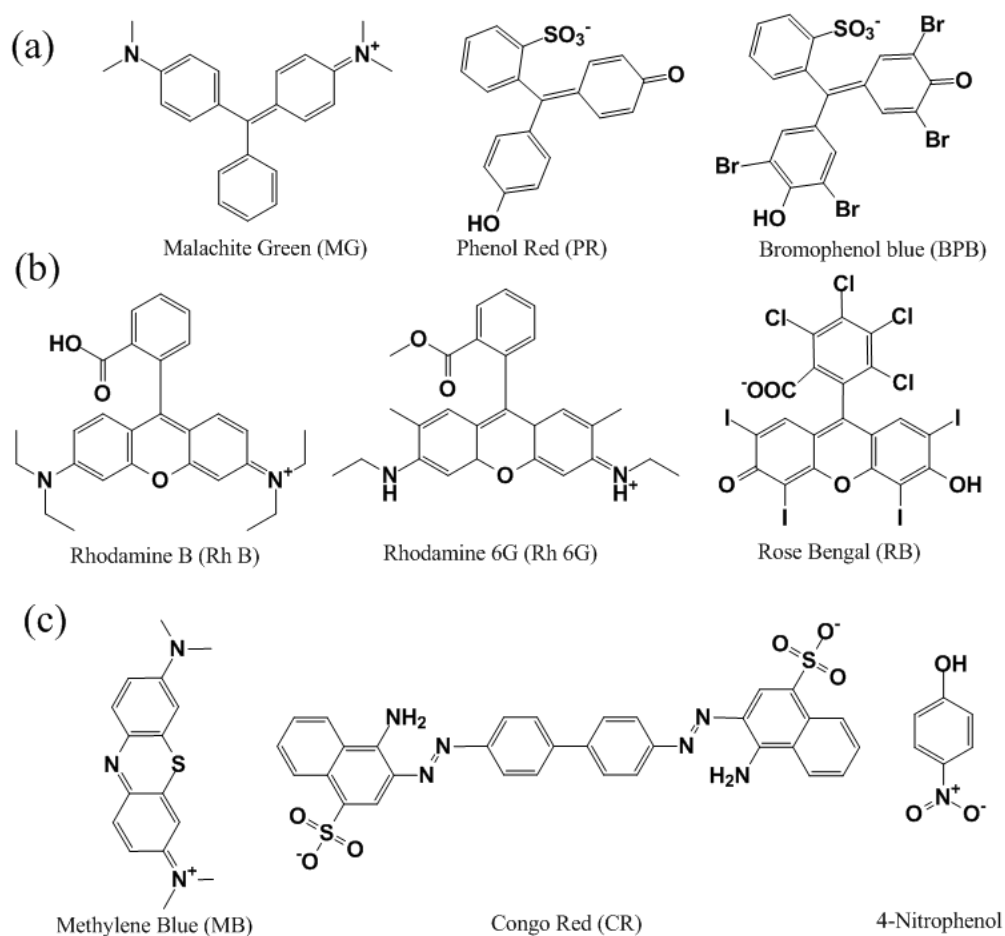


**Figure 5** Structure of dye molecules (a) Triphenyl methane dyes, (b) xanthene dyes and (c) thiazine dye, azo dye and 4-nitrophenol

### 3.2.2 Reduction of triphenyl methane (MG, PR and BPB) dyes

The triaryl methane dyes are intense colored dyes and are used in silk, jute, wool, cotton, paper, leather, and acrylic industries for dyeing purpose. These dyes are grouped into different families depending upon the nature of the substituents present on the aryl groups. In the present study, cationic dye - (diamino derivative-malachite green (MG)) and anionic phenol dyes (hydroxyl derivatives-phenol red (PR), bromophenol blue (BPB)) are selected for reduction.

The chromophoric absorptions ( $\lambda_{\max}$ , nm) of triphenyl methane dyes; MG, PR and BPB are observed at 617, 557 and 592 nm, respectively due to the charge transfer (CT) transitions within the dye molecule (**Table 1**). Notably, the reduction process is followed in the chromophoric adsorption intensities of dyes. When catalytic amount of Pt/AC was added to the reaction mixture, the intensities of the chromophoric peaks were found to decrease, with concomitant appearance/shift of a new peak depending upon the nature of dyes (**Fig.6 a-c**). Besides, the appearance of a new peak at 277 nm for MG (**Fig.6 a**) and a hypsochromic shift of 358 and 284 nm peaks to 339 and 269 nm for PR indicate the formation of leuco form of dyes (**Fig.6 b**). These changes indicate the transformation of quinoid to benzenoid moiety in dyes, as visibly evident from the change in the color of the solution from green, red, blue to colorless for MG, PR and BPB, respectively. The MG, PR and BPB dyes are reduced to their corresponding leuco form (**Table S1**) within 10, 50 and 60 seconds, respectively (**Fig.6 d**). The cationic dye MG undergoes reduction 12 – 16 times faster than the anionic dyes PR and RB. During the reduction process, Pt present on the pores of AC acquires negative charge; hence cationic MG gets adsorbed on Pt nanoparticles and gets reduced at a faster rate than its anionic counterparts. This is reflected in both pseudo rate constant values and  $\Delta G^\ddagger$  values (Table 2).

While comparing the anionic dyes, PR was reduced at a slightly faster rate than BPB, which are adsorbed on the AC surface. This may be due to the presence of bulky  $-\text{SO}_3$ ,  $-\text{OH}$  hydrophilic groups [35] which may hinder the effective adsorption of PR and BPB onto AC surface. Further, presence of  $-\text{Br}$  atoms along with the hydrophilic groups reduced the adsorption of BPB than PR. These observations also correlate with the pseudo rate constant values and  $\Delta G^\ddagger$  values. Moreover, the pseudo first order rate constant ( $k$ ) for triphenyl methane dyes are in the relative order,  $\text{MG} > \text{BPB} > \text{PR}$ . The detailed mechanism is explained in the following topic.

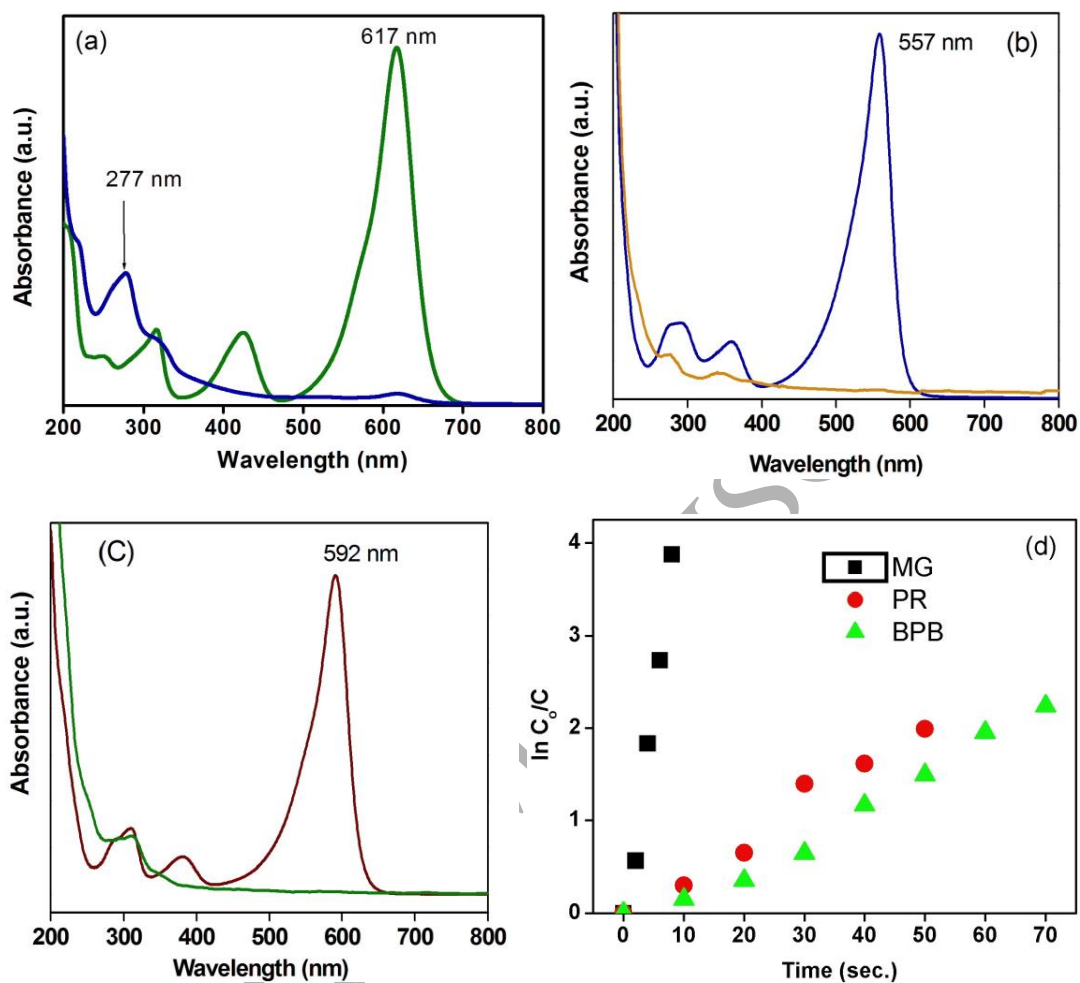


**Figure 6** UV-Visible absorption spectra for before and after reduction with Pt/AC. a) MG, b) PR, c) BPB and d) Plot of  $\ln C_0/C$  vs time ( $R^2 = 0.978-0.998$ )

**Table 2** Catalytic efficiency of Pt/AC for reduction of triphenyl methane dyes

Triphenyl methane dyes	Time of reduction (s)	$k \times 10^2$ ( $s^{-1}$ )	$R^2$	$\Delta G^\#$ ( $KJ mol^{-1}$ )
Malachite green (MG)	10	49.60	0.988	-1737
Phenol red (PR)	60	4.28	0.979	-7865
Bromophenol blue (BPB)	50	3.40	0.978	-8377

### 3.2.3 Reduction of Xanthene (RB, Rh 6G and RhB)

The compounds containing heterocyclic xanthene nucleus are often called as xanthene dyes. These dyes tend to be fluorescent and are used as pigments and also in dyeing and paper industries. Among the various xanthene dyes – Rose Bengal (RB), Rhodamine 6G (Rh 6G) and Rhodamine B (RhB), which contain condensed rings with heteroatoms in the central ring (**Fig.5 b**) were chosen as model reactants. The rhodamine derivatives (Rh 6G, Rh B) are cationic dyes and RB is an anionic dye. The reduction process was followed in the chromophoric absorption ( $\lambda_{max}$ , nm) intensities of Rh B, Rh 6G and RB at 554, 527 and 537 (CT transitions), respectively (**Fig.7 a-c**). The dyes reduced to their corresponding leuco form are shown in the **Table S2**. As expected, the cationic dyes were reduced at a faster rate than the anionic dyes. Among the cationic dyes, Rh B was reduced at a faster rate than its counterpart Rh 6G. This may be due to the presence of sterically crowded ester group at the cationic iminium site, which is also evidenced from the rate constant and  $\Delta G$  values. Slower reactivity of the anionic dye RB may be due to the presence of hydrophobic groups  $-C=O$ ,  $-Cl$  and aromatic groups, which can facilitate desorption from AC surface. In particular, presence of sterically crowded groups in Rh 6G (methyl and ester groups) and RB (bulky halo substituents) at the cationic reaction site may be the reason for the

lower reactivity and desorption from the catalyst surface. This observation is also evidenced from the time taken for complete reduction,  $\Delta G^\ddagger$  and rate constant values (**Table 3**). The pseudo first order rate constants are found to be in the relative order, Rh B > Rh 6G > RB. Tang *et al* has reported the homogeneous adsorption of RhB on CoNP-ordered mesoporous carbon with positive  $\Delta H$  and negative  $\Delta G$  values. Besides, the absorption equilibrium could be reached within 25 min to 60 min [13].

**Table 3** Catalytic efficiency of Pt/AC in reduction of xanthene dyes

Xanthene dyes	Time of reduction (s)	$k \times 10^2$ ( $s^{-1}$ )	$R^2$	$\Delta G^\ddagger$ (KJ mol $^{-1}$ )
Rhodamine B (RhB)	40	5.45	0.988	-7210
Rhodamine 6G (Rh 6G)	70	3.27	0.992	-8475
Rose Bengal (RB)	90	2.89	0.996	-8784

The cationic dye Rh 6G was reduced slower than Rh B due to the presence of sterically crowded methyl and ester groups. These factors cause a decrease in the rate constant for reduction. Further, the RB is an anionic dye with eight halo substituents, besides COOH group may not be strongly adsorbed on Pt/AC catalyst, due to the anionic nature of RB it may be attached to the catalyst support- Pt/AC and hence the rate of reduction is slower than those of Rh B and Rh 6G.

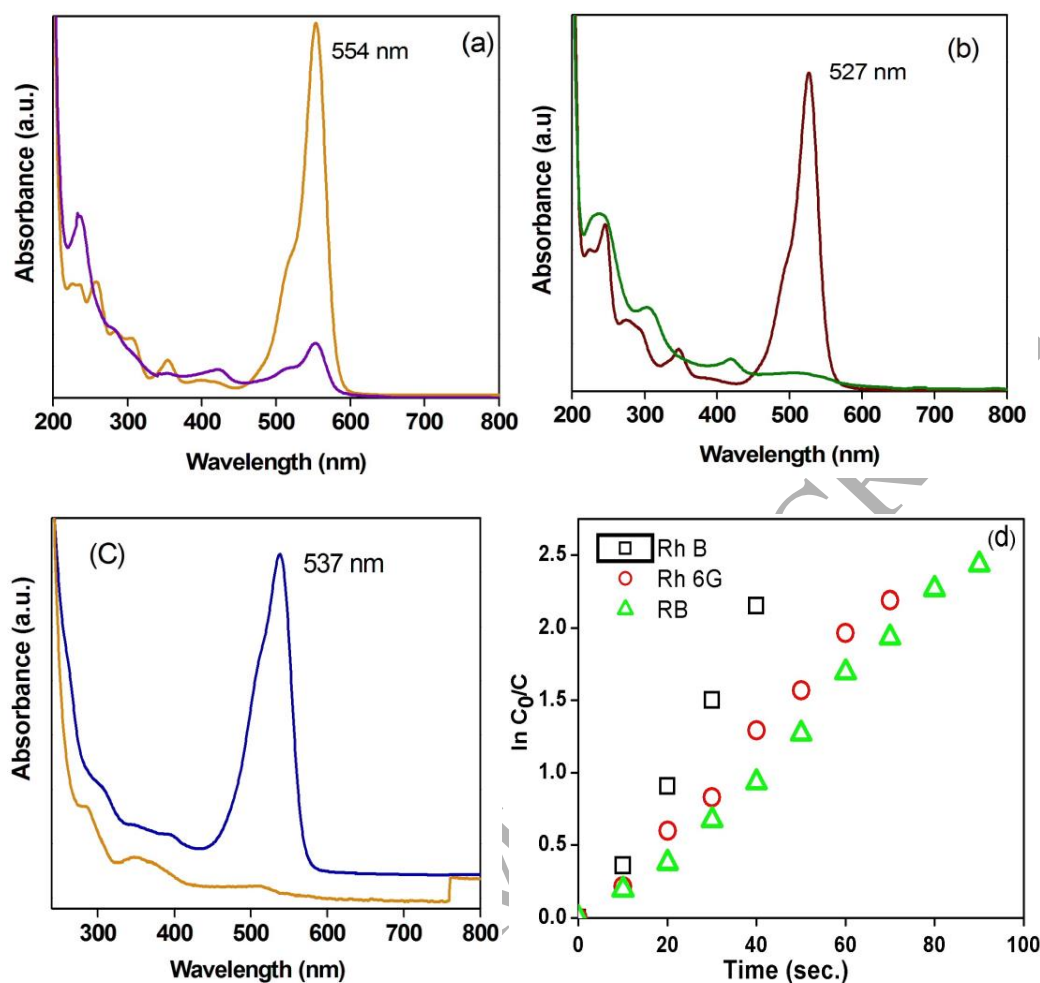


**Figure 7** UV-Visible absorption spectra for before and after reduction with Pt/AC. a) Rh B, b) Rh 6G, c) RB and d) Plot of  $\ln C_0/C$  vs time ( $R^2 = 0.988-0.992$ ).

### 3.2.4 Reduction of thiazine dye (MB), azo dye (CR), and 4-nitrophenol (4-NP)

Azo dyes are class of synthetic organic dyes which contain azo group ( $-N=N-$ ) as chromophore. This functional moiety with variety of colors, are commercially used in textile and dyeing industries. For the reduction, anionic dye congo red (CR) was chosen as model reactant. The reduction process was monitored in the chromophoric absorption ( $\lambda_{max}$ , nm) at 496 nm (**Fig. 8 a**). Since CR is large in structure and contains two azo groups, CR was found to be reduced at a

slower rate (**Fig.8 d**) as expected. The reduction rate constant,  $k$  for CR was estimated be  $2.28 \times 10^2 \text{ s}^{-1}$  (**Table 4**). Further, methylene blue (MB), which contains condensed rings with heteroatoms in the central ring was chosen as thiazine dye for reduction. The cationic MB dye revealed UV-Visible absorption at 665 nm (**Fig.8 b**). Here, the deep blue colour of the solution changed to colorless, which indicated the conversion of MB dye to leuco form and it matched well with the previous reported work on catalytic degradation of MB dye by sodium borohydride in the presence of glutathione coated Ag nanoparticles [36]. MB being cationic in nature underwent faster reduction than anionic dye CR. Presence of two hydrophilic groups  $-\text{SO}_3$ ,  $-\text{NH}_2$  favoured fast desorption thus predominantly favored the reduction. These were also confirmed from the rate constant and  $\Delta G^\ddagger$  values.

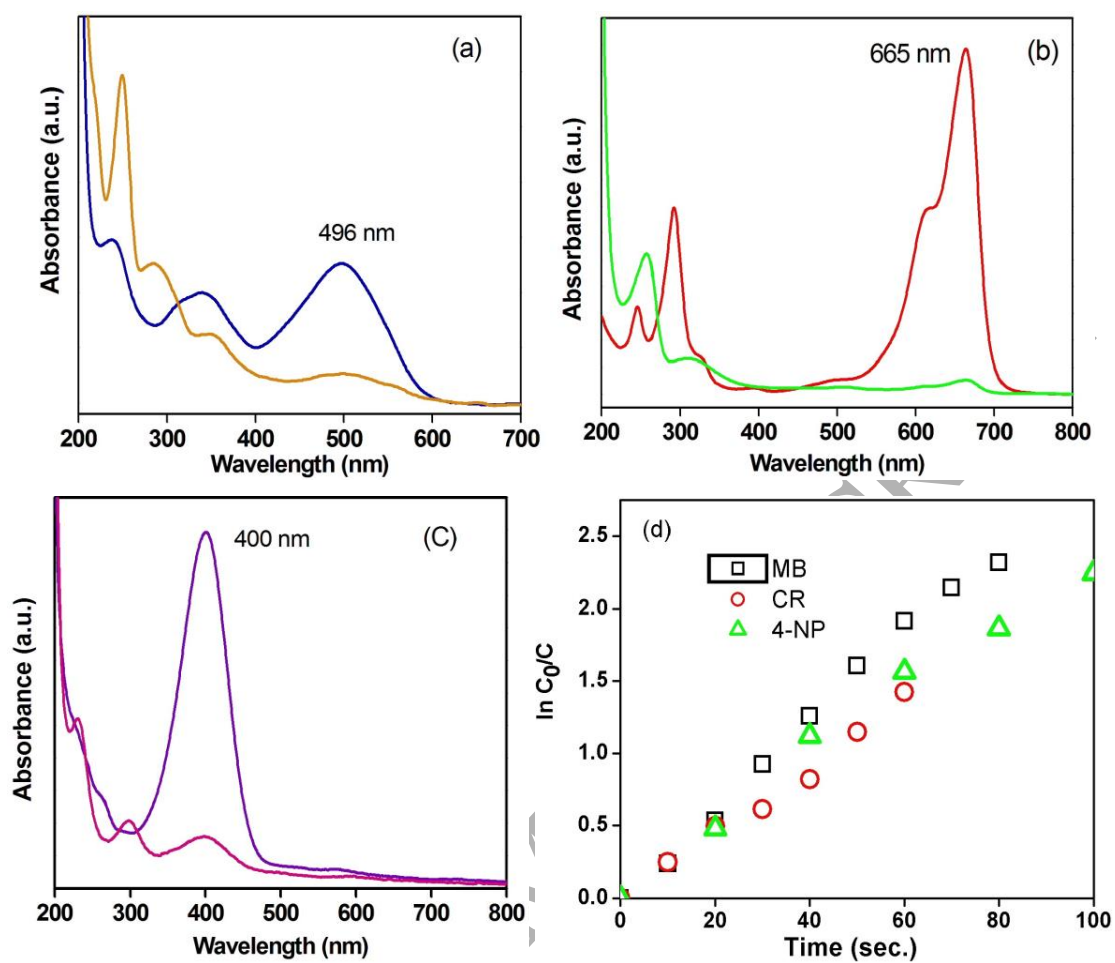


**Figure 8** UV-Visible absorption spectra for before and after reduction with Pt/AC. a) CR, b) MB, c) 4-NP and d) Plot of  $\ln C_0/C$  vs time ( $R^2 = 0.988-0.998$ ).

**Table 4** Catalytic efficiency of Pt/AC catalyst in reduction of methylene blue, congo red dye and 4-nitrophenol

Dye	Time of reduction (s)	$k \times 10^2$ (s <sup>-1</sup> )	R <sup>2</sup>	$\Delta G^\#$ (KJ mol <sup>-1</sup> )
Congo red (CR)	60	2.28	0.989	-9362
Methylene blue (MB)	80	3.08	0.998	-8626
4-Nitrophenol (4-NP)	100	2.26	0.988	-9389

Similarly, the reduction of 4-nitrophenol was followed at the chromophoric absorption ( $\lambda_{\max}$ , nm) peak of 4-nitrophenolate ion at 401 nm [36, 37]. As reduction reaction proceeded, the intensity at 401 nm was found to decrease with simultaneous appearance of new peaks at 300 and 230 nm attributed to the formation of 4-aminophenol (**Fig.8 c**) [37]. The rate constant for the reduction reaction is calculated from the slope of the linearized straight line of the plot of  $\ln C_0/C$  vs time and are tabulated in **Table 4**. The higher reactivity of 4-nitrophenol may be due to the small size, which favored effective binding to the catalyst surface.

In comparison, over Ag nanoparticles 4-NP, methylene blue and eosin Y type dyes are reduced in the presence of sodium borohydride with a faster reduction rate (20 min.) [36]. Nie *et al* have reported Pt supported reduced graphene oxide with 100 % conversion of nitroarenes [29]. Further, the magnetic Fe/Ni nanoparticles doped bimodal mesoporous carbon material could adsorb both cationic dye (methylene blue) and anionic dye (methyl orange) with maximum adsorption capacity of 959.5 mg/g and 849.3 mg/g, respectively [38]. Similarly, Au, Ag and Cu type nanoparticle dispersed ACs were showed about 99 % of dye removal efficiency [9-11]. However, most of these reports discussed about the adsorption based mechanism.

### 3.2.5 Mechanism of reduction process

In all the dye reduction processes, sodium borohydride differs in its reactivity towards different functional groups present on the dye molecule. Often, carbonyl compounds containing carboxylic acids, nitrile and nitro groups as substituents are not tolerable. Particularly, functional groups of triphenyl methane, xanthene and azo dyes are  $-C=O$ ,  $-C=N$  and  $N=N$ , respectively (**Table S4**). Further, the reduction of dyes by sodium borohydride on the surface of Pt/AC has been found to occur in two steps. When Pt/AC was mixed in the solution containing dyes and sodium borohydride, both were simultaneously adsorbed on the surface of the catalyst. Here,  $NaBH_4$  behaves as donor (nucleophile) and dyes as acceptor (electrophile) molecules. As nucleophile will donate electrons to Pt nanoparticles and electrophile will capture from metal nanoparticles, the mechanism of dye reduction follows electron relay from Pt/AC to dyes in the presence of sodium borohydride. Notably, the metal nanoparticles stored the electrons and acted as nanoelectrodes with negative potential [39]. In the reaction, step 1 involves the simultaneous adsorption of dye and sodium borohydride on the surface of the catalyst. The step 2 involves the transfer of electron or hydride from  $BH_4^-$ ---Pt nanoparticles to dyes and desorption of reduced form of dye molecules (Leuco dye) [36, 27]. In general, the reaction proceeds through the following steps



**Scheme 1** The possible mechanism of dye reduction over Pt/AC catalyst

The detailed mechanistic steps for the catalytic reduction of different cationic and anionic dyes by  $NaBH_4$  using Pt/AC are given in the **Scheme S1-S3** and **Figure S2 & S3**.

### 3.2.6 Percentage reduction efficiency and recyclability of dyes over Pt/AC

Successful reduction by Pt/AC catalyst was achieved for all the dyes irrespective of their chemical structure. The percentage of reduction is approximately 90% for all types of dyes (**Fig.9 a**). The reduction efficiency of Pt/AC sample was examined for all the dyes collected at five cycles with same experimental conditions. After each cycle the catalyst was recovered by decantation, washed with deionised water, dried and a fresh solution of dyes with sodium borohydride was added for next cycle. The percentage reduction of dyes for the five cycles with similar activity is shown in **Fig. 9 b**. Interestingly, the catalytic efficiency of the catalyst was maintained without any loss of activity due to the inherent stabilization of Pt nanoparticles within the pores of AC support.

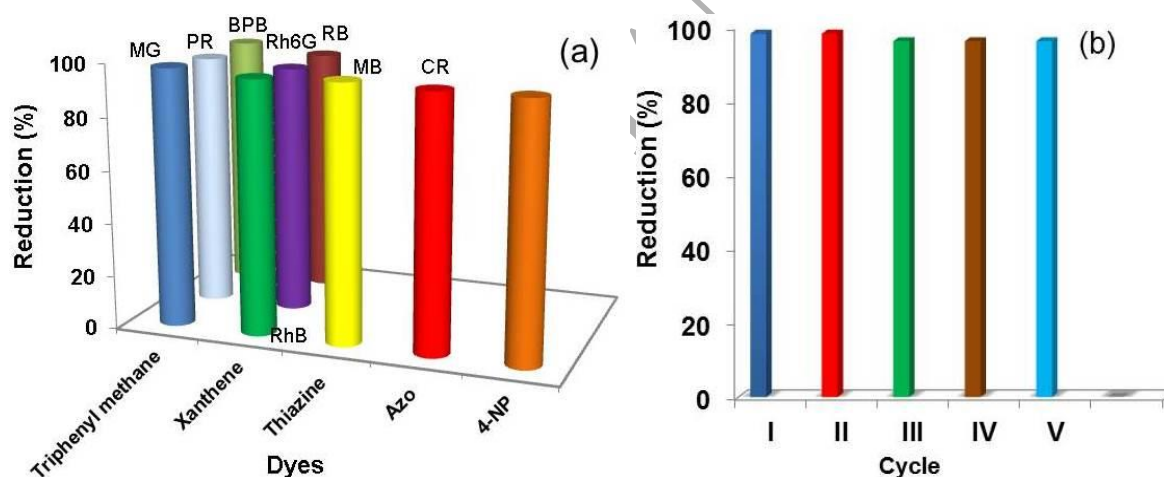


**Figure 9** (a) percentage reduction efficiency for different dyes and (b) reusability of Pt/AC catalyst for dye reductions

### 3.2.7 Relationship between reduction mechanisms and dye characteristics

In order to determine the relationship between reduction mechanisms and dye characteristics, dyes were grouped according to their chemical structures (class of dyes). Pt/AC successfully reduced all dyes irrespective of their chemical structure. The percentage of reduction is approximately 90%

(Fig. 9 a) for all types of dyes. The reduction of dyes by sodium borohydride seems to follow two major steps, reduction and adsorption, which work differently during reduction process. Though both mechanisms occur during reduction, adsorption is the predominant mechanism, which determines the rate of dye reduction. Negative value of  $\Delta G^\ddagger$  implies that the adsorption process from dye to catalyst is spontaneous and thermodynamically favorable. The order of reactivity of dyes corroborates with the  $\Delta G^\ddagger$  values.

## Conclusion

In summary, 5% Pt dispersed AC catalyst synthesized from bio-waste has been prepared. The synthesized catalyst was confirmed by many characterization techniques. Here the groundnut carbon holds two-fold advantage, as it will act not only as adsorbent but also provide better stabilization for Pt nanoparticles. The Pt nanoparticles are well dispersed over the surface. The catalytic reduction performance of Pt/AC showed an excellent catalytic activity towards the reduction of various dyes (triphenyl methane, xanthene, thiazine and azo dyes) in the presence of  $\text{NaBH}_4$ . Mainly, the dye reduction reactions followed the pseudo unimolecular kinetics. Furthermore, the catalyst was found to be quite fast in reducing (below 2 minutes) the dyes to their corresponding leuco forms. The rate constant ( $k$ ) and  $\Delta G^\ddagger$  values varied based on the size, diffusion, nature (anionic/cationic) and functional groups present in the dye molecules. The reduction of dyes by sodium borohydride appears to follow two major steps, reduction and adsorption, which work differently during reduction process. Though both mechanisms occur or responsible for the reduction, adsorption is the predominant mechanism, which determines the rate of dye reduction. Moreover, negative value of  $\Delta G^\ddagger$  implies that the adsorption process from dye to catalyst is thermodynamically favorable. The order of reactivity of triphenyl methane

(MG > PR > BPB), xanthene dyes (Rh B > Rh 6G > RB), thiazine (MB), azo dye (CR) and 4-NP, which was also substantiated by the  $\Delta G^\ddagger$  values. This work may be helpful in developing the different dye reduction processes under suitable reaction conditions.

### **Acknowledgment**

The authors SAAV and BV gratefully acknowledge Department of Science and Technology (DST), India for setting up the National Center for Catalysis Research (NCCR), IIT Madras.

### **Appendix A. Supplementary material**

Supplementary data to this article can be found online at.

## Captions

Figure 1 PXRD patterns of Pt/AC catalyst

Figure 2 (a), (b) SEM and (c), (d) TEM images of Pt/AC catalyst

Figure 3 FTIR of Pt/AC catalyst

Figure 4 (a) C1s and (b) Pt 4f core level XPS spectrum of Pt/AC catalyst

Figure 5 Structure of dye molecules (a) Triphenyl methane dyes (MG, PR & BPB), (b) Xanthene dyes (RhB, Rh6G & RB), and (c) thiazine dye (MB), Azo dye (CR), 4-Nitrophenol

Figure 6 UV-Visible absorption spectra for before and after reduction with Pt/AC. a) MG, b) PR, c) BPB and d) Plot of  $\ln C_0/C$  vs time ( $R^2 = 0.978-0.998$ )

Figure 7 UV-Visible absorption spectra for before and after reduction with Pt/AC. a) Rh B, b) Rh 6G, c) RB, d) Plot of  $\ln C_0/C$  vs time ( $R^2 = 0.988-0.992$ ).

Figure 8 UV-Visible absorption spectra for before and after reduction with Pt/AC. a) CR, b) MB, c) 4-NP, d) Plot of  $\ln C_0/C$  vs time ( $R^2 = 0.988-0.998$ ).

Figure 9 (a) Percentage reduction efficiency for different dyes (b) reusability of Pt/AC catalyst for the dye reductions.

Table 1 Selected dyes their examples, nature and UV-Visible absorbance wavelength

Table 2 Catalytic efficiency of Pt/AC for reduction of triphenyl methane dyes

Table 3 Catalytic efficiency of Pt/AC in reduction of xanthene dyes

Table 4 Catalytic efficiency of Pt/AC catalyst in reduction of methylene blue, congo red dye and 4-nitrophenol

**Reference**

- [1] Sokolowska-Gajda. Synthetic dyes based on environmental considerations. *Dye Pigment*, 30 (1996) 1–20.
- [2] M. T. Yagub, T. K. Sen, S. Afroze, H.M. Ang, Dye and its removal from aqueous solution by adsorption: A review, *Adv Colloid Interfac*, 209 (2014) 172-184.
- [3] S. C. Smith, D. F. Rodrigues, Carbon-based nanomaterials for removal of chemical and biological contaminants from water: A review of mechanisms and applications, *Carbon*, 91 (2015) 122–143.
- [4] C.R. Holkar, A. J. Jadhav, D.V. Pinjari, N. M. Mahamuni, A. B. Pandit, A critical review on textile wastewater treatments: Possible approaches, *J Environ Manage*, 182 (2016) 351–366.
- [5] V. Gupta, Application of low-cost adsorbents for dye removal—a review. *J Environ Manage*, 90 (2009) 2313–42.
- [6] L.R. Radovic, F. Rodriguez-Reinoso, in: P.A. Throver (Ed.), *Chemistry and Physics of Carbon*, vol. 25, Dekker, New York, 1997, p. 243.
- [7] J. R.-Utrilla, M. Sanchez-Polo, V. Gomez-Serrano, P. M. Alvarez, M.C.M. Alvim-Ferraz, J.M. Dias, Activated carbon modifications to enhance its water treatment applications. An overview, *J Hazard Mater*, 187 (2011) 1-23.
- [8] H. Karimi, S. Mousavi, B. Sadeghian, Silver nanoparticle loaded on activated carbon as efficient adsorbent for removal of methyl orange, *Indian J Sci Technol*, 5 (2012) 2346-2353.
- [9] X. Yang, P.-F. Tian, C. Zhang, Y.-q. Deng, J. Xu, J. Gong, Y.-F. Han, Au/carbon as Fenton-like catalysts for the oxidative degradation of bisphenol A, *Appl Catal B-Environ*, 134–135 (2013) 145–152.
- [10] J. Pal, M. K. Deb, D. K. Deshmukh, D. Verma, Removal of methyl orange by activated carbon modified by silver nanoparticles, *Appl Water Sci*, 3 (2013) 367–374.
- [11] M. Ghaedi, E. Shojaeipour, A.M. Ghaedi, R. Sahraei, Isotherm and kinetics study of malachite green adsorption onto copper nanowires loaded on activated carbon: Artificial neural network modeling and genetic algorithm optimization, *Spectrochim Acta A*, 142 (2015)135-149.
- [12] R. Wojcieszak, M. Zieliński, S. Monteverdi, M.M. Bettahar, Study of nickel

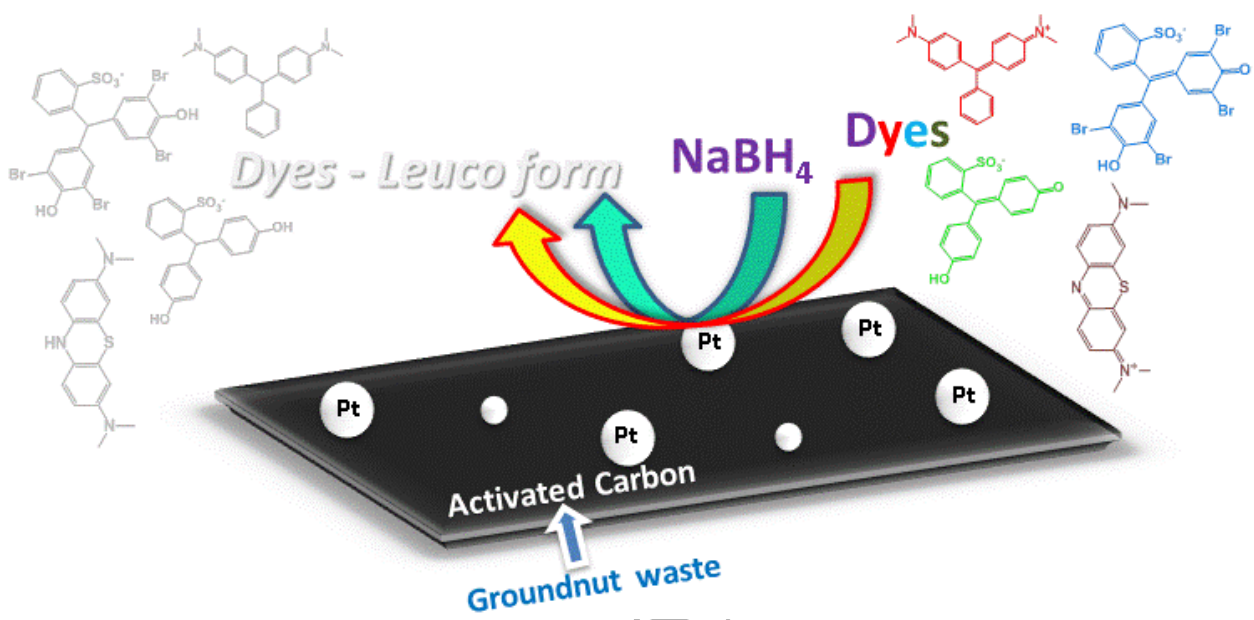
- nanoparticles supported on activated carbon prepared by aqueous hydrazine reduction, *J Colloid Interf Sci*, 299 (2006) 238–248.
- [13] L. Tang, Y. Cai, G. Yang, Y. Liu, G. Zeng, Y. Zhou, S. Li, J. Wang, S. Zhang, Y. Fang, Y. He, Cobalt nanoparticles-embedded magnetic ordered mesoporous carbon for highly effective adsorption of rhodamine B, *Appl Surf Sci*, 314 (2014) 746–753.
- [14] Z.-S. Liu, J.-Y. Chen, Y.-H. Peng, Activated carbon fibers impregnated with Pd and Pt catalysts for toluene removal, *J Hazard Mater*, 256-257 (2013) 49-55.
- [15] M.A. Álvarez-Montero, L.M. Gómez-Sainero, A. Mayoral, I. Diaz, R.T. Baker, J.J. Rodriguez, Hydrodechlorination of chloromethanes with a highly stable Pt on activated carbon catalyst, *J Catal*, 279 (2011) 389–396.
- [16] M.C.M. Pérez, C.S.M. deLecea, A.L. Solano, Platinum supported on activated carbon cloths as catalyst for nitrobenzene hydrogenation, *Appl Catal A*, 151 (1997) 461–475.
- [17] I.M. Vilella, S.R. de Miguel, O.A. Scelza, Study of the performance of Pt catalysts supported on activated carbon felt and granular carbon for nitrobenzene hydrogenation, *Chem Eng J*, 114 (2005) 33–38.
- [18] M. J. Ahmed, A. A. H. Kadhum, Hydrogenation of D-fructose over activated charcoal supported platinum catalyst, *J Taiwan Inst Chem E*, 42 (2011) 114–119.
- [19] M. A. Yahya, Z. Al-Qodah, C.W. Z. Ngah, Agricultural bio-waste materials as potential sustainable precursors used for activated carbon production: A review, *Renew Sust Energ Rev*, 46 (2015) 218–235.
- [20] O. Ioannidou, A. Zabaniotou, Agricultural residues as precursors for activated carbon production—A review, *Renew Sust Energ Rev*, 11 (2007) 1966–2005.
- [21] P. Pang, F. Yan, M. Chen, H. Li, Y. Zhang, H. Wang, Z. Wu, W. Yang, Promising biomass-derived activated carbon and gold nanoparticle nanocomposites as a novel electrode material for electrochemical detection of rutin, *RSC Adv*, 6 (2016) 90446-90454.
- [22] C.E. Gimba, A.A. Salihu, J.A. Kagbu, M. Turoti, A.U. Itodo, A.I. Sariyya. Study of pesticide (Dichlorvos) removal from aqueous medium by *Arachishypogaea* (groundnut shell) using GC/MS. *World Rur Observ*, 2 (2010) 1–9.
- [23] R. Malik, D.S. Ramteke, S.R. Wate, Adsorption of malachite green on groundnut shell waste based powdered activated carbon, *Waste Manage*, 27 (2007) 1129–1138.

- [24] S. Sareen, V. Mutreja, B. Pal, S. Singh, Homogeneous dispersion of Au nanoparticles into mesoporous SBA-15 exhibiting improved catalytic activity for nitroaromatic reduction, *Micropor Mesopor Mat*, 202 (2015) 219–225.
- [25] A.K. Sinha, M. Basu, S. Sarkar, M. Pradhan, T. Pal, Synthesis of gold nanochains via photoactivation technique and their catalytic applications, *J Colloid Interf Sci*, 398 (2013) 13–21.
- [26] X. Wang, J. Fu, M. Wang, Y. Wang, Z. Chen, J. Zhang, J. Chen, Q. Xu, Facile synthesis of Au nanoparticles supported on polyphosphazene functionalized carbon nanotubes for catalytic reduction of 4-nitrophenol, *J Mater Sci*, 49 (2014) 5056–5065.
- [27] J. Li, Y.-h. Ni, C. Liu, L. Zhang, Noncovalent assembly of the carbon nanofibers/Au nanocomposite and its application in 4-Nitrophenol Reduction, *J Clust Sci*, 26 (2015) 1547–1556.
- [28] E. Blanco, P. Atienzar, P. Hernandez and C. Quintan, The Langmuir–Hinshelwood approach for kinetic evaluation of cucurbit[7]uril-capped gold nanoparticles in the reduction of the antimicrobial nitrofurantoin, *Phys Chem Chem Phys*, 2017, 19, 18913 - 18923.
- [29] R. Nie, J. Wang, L. Wang, Y. Qin, P. Chen, Z. Hou, Platinum supported on reduced graphene oxide as a catalyst for hydrogenation of nitroarenes, *Carbon*, 50 (2012) 586–5966.
- [30] F. Sen, S. Sen, G. Gokagac, Efficiency enhancement of methanol/ethanol oxidation reactions on Pt nanoparticles prepared using a new surfactant, 1,1-dimethyl heptanethiol, *Phys Chem Chem Phys*, 13 (2011) 1676–1684.
- [31] H. X. Huang, S. X. Chen, C. Yuan, Platinum nanoparticles supported on activated carbon fiber as catalyst for methanol oxidation, *J Power Sources*, 175 (2008) 166–174.
- [32] S. Karthikeyan, R. Boopathy, G. Sekaran, In situ generation of hydroxyl radical by cobalt oxide supported porous carbon enhance removal of refractory organics in tannery dyeing wastewater, *J Colloid Interf Sci*, 448 (2015) 163–174.
- [33] A.A. Olajire, J.J. Abidemi, A. Lateef, N.U. Benson, Adsorptive desulphurization of model oil by Ag nanoparticles-modified activated carbon prepared from brewer's spent grains, *J Environ Chem Eng*, 5 (2017) 147–159.
- [34] F. S¸ en, G. Gokag¸ ac¸ u, Different sized platinum nanoparticles supported on carbon: An XPS study on these methanol oxidation catalysts, *J Phys Chem C*, 111

(2007) 5715-5720.

- [35] Z. Shen, W. Wang, J. Jia, J. Ye, X. Feng, A. Peng, Degradation of dye solution by an activated carbon fiber electrode electrolysis system, *J Hazard Mater*, 84 (2001) 107–116.
- [36] R. Rajamanikandan, K. Shanmugaraj, M. Ilanchelian, Concentration dependent catalytic activity of Glutathione coated silver nanoparticles for the reduction of 4-nitrophenol and organic dyes, *J Clust Sci*, 28 (2016) 1009-1023.
- [37] B.K. Ghosh, S. Hazra, B. Naik, N. N. Ghosh, Preparation of Cu nanoparticle loaded SBA-15 and their excellent catalytic activity in reduction of variety of dyes, *Powder Technol.*, 269 (2015) 371–378.
- [38] Y. Liu, G. Zeng, L. Tang, Y. Cai, Y. Pang, Y. Zhang, G. Yang, Y. Zhou, X. He, Y. He, Highly effective adsorption of cationic and anionic dyes on magnetic Fe/Ni nanoparticles doped bimodal mesoporous carbon, *J Colloid Interf Sci*, 448, (2015) 451- 459.
- [39] J.-P. Deng, W.-C. Shih, C.-Y. Mou, Electron transfer-induced hydrogenation of anthracene catalyzed by gold and silver nanoparticles, *J Phys Chem C*, 111 (2007) 9723–9728.

## Graphical abstract



ACCEPTED MA